# 

Stefanie M. Hauck†\*\*, Johannes Dietter†, Roxane L. Kramer¶, Florian Hofmaier¶, Johanna K. Zipplies¶, Barbara Amann¶, Annette Feuchtinger§, Cornelia A. Deeg¶‡‡, and Marius Ueffing†∥‡‡

Autoimmune uveitis is a blinding disease presenting with autoantibodies against eye-specific proteins as well as autoagressive T cells invading and attacking the immuneprivileged target tissue retina. The molecular events enabling T cells to invade and attack the tissue have remained elusive. Changes in membrane protein expression patterns between diseased and healthy stages are especially interesting because initiating events of disease will most likely occur at membranes. Since disease progression is accompanied with a break-down of the blood-retinal barrier, serum-derived proteins mask the potential target tissue-related changes. To overcome this limitation, we used membrane-enriched fractions derived from retinas of the only available spontaneous animal model for the disease equine recurrent uveitis, and compared expression levels by a label-free LC-MSMS-based strategy to healthy control samples. We could readily identify a total of 893 equine proteins with 57% attributed to the Gene Ontology project term "membrane." Of these, 179 proteins were found differentially expressed in equine recurrent uveitis tissue. Pathway enrichment analyses indicated an increase in proteins related to antigen processing and presentation, TNF receptor signaling, integrin cell surface interactions and focal adhesions. Additionally, loss of retina-specific proteins reflecting decrease of vision was observed as well as an increase in Müller glial cell-specific proteins indicating glial reactivity. Selected protein candidates (caveolin 1, integrin alpha 1 and focal adhesion kinase) were validated by immunohistochemistry and tissue staining pattern pointed to a significant increase of these proteins at the level of the outer limiting membrane which is part of the outer blood-retinal barrier. Taken together, the mem-

brane enrichment in combination with LC-MSMS-based label-free quantification greatly increased the sensitivity of the comparative tissue profiling and resulted in detection of novel molecular pathways related to equine recurrent uveitis. *Molecular & Cellular Proteomics 9:* 2292–2305, 2010.

Autoimmune uveitis is a disease with recurrent attacks of the inner eye, eventually leading to blindness (1). Activated, autoaggressive T cells specific for retinal autoantigens cross the blood-retinal barrier and are responsible for the tissue destruction (2). To date, the molecular pathomechanisms of blood-retinal barrier crossing of the events causing disease progression as well as the causative events for relapses remain as yet unresolved. The spontaneous animal model equine recurrent uveitis (ERU)1 (3) enabled us to undertake several studies comparing diseased versus healthy condition by proteomic analyses utilizing retina, vitreous and serum samples from horses (4). As a result, we have shown that retinal Mueller cells are players in the pathogenesis of the disease as they transform into a gliotic phenotype-decreasing expression of glutamine synthetase and pigment epitheliumderived factor (PEDF) and simultaneously start expressing interferon gamma (5). This observation is complemented by a quantitative comparison of serum samples with twodimensional-DIGE, where PEDF was also significantly downregulated in ERU cases (6).

However, because a hallmark of the disease is the breakdown of the blood-retinal barrier (BRB), the tissue is flooded with the compounds of serum to an increasing extent along with disease severity. This is reflected by an increasing de-

Published, MCP Papers in Press, July 4, 2010 DOI 10.1074/mcp.M110.001073

From the †Department of Protein Science, and the §Institute of Pathology, Helmholtz Zentrum München - German Research Center for Environmental Health (GmbH), Neuherberg, Germany; ¶Institute of Animal Physiology, Department for Veterinary Sciences, Ludwig-Maximilians University, München, Germany; ∥Center for Ophthalmology, Institute of Ophthalmic Research, University Tübingen, Tübingen, Germany Received May 21, 2010, and in revised form, June 30, 2010.

 $<sup>^1</sup>$  The abbreviations used are: BRB, blood-retinal barrier; CAV1, Caveolin 1; ECM, extracellular matrix; ERU, equine recurrent uveitis; FAK, focal adhesion kinase; FN, fibronectin; GO, gene onthology; IFN $\gamma$ , interferone gamma; ITGA1, integrin alpha 1 (synonyms: PELO, CD49a); ITGB1, integrin beta 1; OLM, outer limiting membrane; PEDF, pigment epithelium-derived factor; TGF $\beta$ , transforming growth factor beta; TNF $\alpha$ , tumor necrosis factor alpha; TMD, transmembrane domain; VEGF, vascular endothelial growth factor; VTN, vitronectin.

tection of the major components from serum such as albumin, transferring, and immunoglobulins as observed in classical 2D-gel based proteomics comparisons (5) from total retinal lysates. To quantitatively compare the composition of the target tissue itself, we decided to enrich the membrane and insoluble protein fractions from healthy and diseased tissue and directly subject those enriched tissue compartments to mass spectrometric identifications. Additionally, changes in the membrane proteome containing cellular and tissue surface proteins are especially interesting for understanding early events in the pathogenesis of this autoimmune disease because it involves auto-aggressive T cells entering and attacking the retinal structures and surface changes can potentially trigger these processes (7).

In view of the fact that for such a large animal model as the horse, metabolic stable isotope labeling techniques such as stable isotope labeling with amino acids in cell culture are not applicable and because isotope-coded protein labeling proved too ineffective for small protein amounts (Hauck, unpublished observations), we used label-free quantification based on peptide peak intensity comparisons for differential profiling of membrane-enriched fractions.

## **EXPERIMENTAL PROCEDURES**

Collection of ERU Cases and Controls—ERU was diagnosed according to clinical criteria as described by Deeg et al.(8). A total of 15 ERU cases and 15 healthy controls were used for this study, including identification of differentially expressed membrane protein candidates and validation by immunohistochemistry. Eyes (both healthy and ERU) were sampled from horses that were patients in the Equine Clinic and had to be euthanized due to reasons unrelated to this study. A minor caseload of ERU eyes came from therapeutically enucleated eyes. Healthy controls were matched in sex and age. Retinas were dissected from the posterior eyecups directly after enucleation and were immediately stabilized with protease inhibitors (Roche) and stored at -20 °C until further processing. For immunohistochemistry, collected eyes were fixed with Bouin's solution (Sigma), embedded in paraffin (Micron), and sectioned (see more details below).

Sample Preparation - Membrane proteins from retinal tissue were extracted as described (9) with the following adaptations. Forty miligrams of frozen retinal tissue were homogenized in 3 ml of high salt buffer (2 M NaCl, 10 mm HEPES-NaOH, pH 7.4, 1 mm EDTA, complete protease inhibitors) using an IKA Ultra Thurax blender. The raw lysate was centrifuged at 17,500 g, at 4 °C for 30 min. The resulting pellet was homogenized with 1.5 ml carbonate buffer (0.1 M Na<sub>2</sub>CO<sub>3</sub>, pH 11.3, 1 mm EDTA, 1 × complete), incubated on ice for 30 min, and collected by centrifugation (17,500 g, 30 min at 4 °C). The pelleted proteins were re-extracted once more with carbonate buffer as above. After centrifugation, the pellet was homogenized with 3 ml urea buffer (4 m urea, 100 mm NaCl, 10 mm HEPES/NaOH, pH 7.4, 1 mм EDTA, 1  $\times$  complete) and centrifuged (17,500 g, 30 min at 4 °C). In contrast to the previous published protocol (9), resulting membrane protein pellets were directly used for tryptic digests. From each tissue (healthy and ERU), three 40-mg portions were processed in parallel (technical replicates). All soluble fractions were combined, dialyzed for 12 h against 10 mm Tris pH 7.5, and proteins collected by acetone precipitation as described before (10) and used for SDS-PAGE and Western blots only (see below).

Membrane protein pellets were each solubilized in 36  $\mu$ l of ammoniumbicarbonate and 4  $\mu$ l of RapiGest<sup>TM</sup> surfactant (Waters, Milford, MA),

denatured by addition of 2  $\mu$ l of 100 mm DTT and heated for 10 min to 60 °C, cooled, and alkylated by addition of 2  $\mu$ l of 300 mm iodoacetamid for 30 min in the dark at room temperature. Trypsin was added (5  $\mu$ l, 0.5 mg/ml) and samples were incubated at 37 °C for 16 h, followed by addition of 2  $\mu$ l of trypsin and incubation for additional 20 h. Samples were acidified by addition of 3  $\mu$ l of concentrated hydrogen chloride (HCl) and centrifuged (16,000 g for 30 min at 4 °C). Soluble phase was retrieved and used immediately for LC-MSMS analysis.

Mass Spectrometry-LC-MSMS analysis was performed on an Ultimate3000 nano HPLC system (Dionex, Sunnyvale, CA) online coupled to a LTQ OrbitrapXL mass spectrometer (Thermo Fisher Scientific) by a nano spray ion source. Samples originating from in-solution digests of membrane fractions of retinal tissue were acidified with TFA and automatically loaded to the HPLC system equipped with a nano trap column (100  $\mu$ m i.d.  $\times$  2 cm, packed with Acclaim PepMap100 C18, 5  $\mu$ m, 100 Å, Dionex) at a flow rate of 30  $\mu$ l/minute in 5% buffer B (80% acetonitrile, 0.1% FA in HPLC-grade water) and 95% buffer A (5% acetonitrile, 0.1% FA in HPLC-grade water). After 5 min, the peptides were eluted and separated on the analytical column (75  $\mu$ m i.d.  $\times$  15 cm, Acclaim PepMap100 C18, 3  $\mu$ m, 100Å, Dionex) by a gradient from 5% to 50% of buffer B at 300 nL/minute flow over 140 min. Remaining peptides were eluted by a short gradient from 50% to 100% buffer B in 5 min. The eluting peptides were analyzed by the LTQ OrbitrapXL. From the high resolution MS prescan, the five most intense peptide ions were selected for fragment analysis in the linear ion trap if they exceeded an intensity of at least 200 counts and if they were at least doubly charged. The normalized collision energy for CID was set to a value of 35 and the resulting fragments were detected with normal resolution in the linear ion trap. The lock mass option was activated, and the background signal with the mass of 445.120020 was used as lock mass (11). Every ion selected for fragmentation was excluded for 30 s by dynamic exclusion.

Label-Free Peptide Quantifications-The acquired spectra were loaded (Thermo raw files) to the Progenesis software (version 2.5, Nonlinear) for label free quantification. Profile data of the MS scans were transformed to peak lists with Progenesis LC-MS using a proprietary algorithm. This method uses wavelet-based filtering to smooth the peak envelopes and identify noisy areas, i.e. areas deemed to contain no ion peaks. Peaks are then modeled in nonnoisy areas to record their peak m/z value, intensity, abundance (area under the peak) and m/z width. MS/MS spectra were transformed similarly and then stored in peak lists comprising m/z and abundance. After selecting one sample as a reference, the retention times of all other samples within the experiment are aligned by manually creating three to five landmarks followed by automatic alignment of all retention times to maximal overlay of the 2D feature maps. Features with only one charge or more than seven charges are masked at this point and excluded from further analyses. After alignment and feature exclusion, samples were divided into the appropriate groups (healthy and ERU), and raw abundances of all features were normalized. Normalization corrects for factors resulting from experimental variation and was automatically calculated over all features in all samples. It results in a unique factor for each sample that corrects all features in the sample in a similar way for experimental variation. After normalization, statistical analysis was performed using transformed ("log-like" arcsinh(.)function) normalized abundances for one-way analysis of variance (ANOVA) calculations of all detected features. No minimal thresholds were set neither for the method of peak picking nor selection of data to use for quantification. Co-detection across all runs ensures that abundance data used for relative quantification is obtained for every peptide ion in every run resulting in data variance that is representative of the full dataset. Principal component analysis of all identified peptides revealed that the peptides cluster according

to the groups and 41.5% of the peptides have a power > 0.8. For quantification, all peptides (with Mascot score  $\geq$  30 and p < 0.01) of an identified protein were included and the total cumulative abundance was calculated by summing the abundances of all peptides allocated to the respective protein. Calculations of the protein p value (one-way ANOVA) were then performed on the sum of the normalized abundances across all runs. ANOVA values of  $p \leq$  0.05 and additionally regulation of  $\geq$  2-fold or  $\leq$  0.5-fold were regarded as significant for all further results.

After quantification of peptides, those features not having an MS/MS scan from the initial samples run were exported to Excel (Microsoft) and used as an inclusion list for a replicate run of samples on the Orbitrap. Resulting raw data files were aligned to the experiments in Progenesis and additional MS/MS scans resulting from these measurements were added to the previous ones; however, the original quantifications and statistics were not changed.

Database Search and Protein Identification-All MS/MS spectra were exported from the Progenesis software as Mascot generic file (mgf) and used for peptide identification with Mascot (version 2.2) in the Ensembl database for horse (Equus caballus; EquCab2.56.pep, downloaded from ftp://ftp.ensembl.org/pub/current\_fasta/equus\_ caballus/pep/) containing a total of 22,640 protein sequences. Search parameters used were: 10 ppm peptide mass tolerance and 1-Da fragment mass tolerance, one missed cleavage allowed, carbamidomethylation was set as fixed modification and methionine oxidation, as well as phosphorylation of tyrosine, serine, and threonine were allowed as variable modifications. A Mascot-integrated decoy database search calculated a false discovery of ≤ 3.55% when searching was performed on the concatenated mgf files with an ion score cut-off of 30 and a significance threshold of  $p \le 0.01$ . Only peptides with ion scores of 30 and above and only proteins with at least one unique peptide ranked as top candidate (bold red in Mascot) were considered and re-imported into Progenesis software. All protein identifications are listed in supplemental Table 1 (separated into a list containing all proteins and another one containing only proteins with two or more unique peptides), all peptide identifications are listed in supplemental Table 6. Identifications and quantifications of proteins based on only one peptide have to be accepted with care; however, they were considered for the explorative phase (pathway enrichment and protein network analyses) in order not to overlook anything (eg, false negatives). False positives would be identified and deleted in the later validation phase of the workflow.

# Gene Ontology, Pathway Enrichment Analysis and Protein Network Analysis

Pathway Enrichment Analysis - We first searched the corresponding gene symbol for every identified protein in the Ensembl database (ftp://ftp.ensembl.org/pub/current\_embl/equus\_caballus/). If a gene symbol was not available, the gene symbol of the human orthologue was used. With the resulting gene list, pathway enrichment analyses were performed, separately for the upregulated and downregulated genes. A gene was regarded as upregulated or downregulated if the relation of relative cumulative peptide intensities between healthy and ERU was ≤ 0.5 (≥ 2.0) and the corresponding p value calculated with the ANOVA test was  $\leq$  0.05. In particular, we have used the overrepresentation analysis tool of the ConsensusPathDB program (version 12) (12) to obtain the overrepresented pathways from both gene sets. The complete set of identified genes has been taken as background list for the analyses. In Tables I and II, the overrepresented pathways derived from the downregulated and upregulated genes are listed. In addition to the information already supplied by the ConsensusPathDB program, we also included genes belonging to a respective pathway which were either not regulated or regulated in the opposite direction.

Protein Classification With Gene Ontolog)—Identified proteins were used for Gene Ontology (GO) term annotations "cellular component" based on Homo sapiens with BiNGO (BiNGO-2.31) (13). 508 proteins could be allocated to the GO term "membrane" and based on this, percent membrane proteins were calculated considering GO terms "plasma membrane," "mitochondrial envelope," "endoplasmic reticulum membrane," "vesicle," and "nuclear membrane" (see supplemental Table 5). TMHMM 2.0 (http://www.cbs.dtu.dk/services/TMHMM/) was used for the prediction of transmembrane domains (14).

Protein Network Analysis—Gene symbols for identified upregulated and downregulated proteins ( $p \le 0.05$  and  $\ge 2$ -fold or  $\le 0.5$ -fold) as well as unregulated proteins (p > 0.05 and regulation between 2-and 0.5-fold) were further analyzed with the Search Tool for Retrieval of Interacting Genes/Proteins (STRING) tool version 8.2 (http://string.embl.de) (15). The protein interaction maps were created by allowing for experimental evidence as well as for the following predicted functional links: co-occurrence, co-expression, databases, and textmining. Stronger associations are represented by thicker lines and minimal required confidence was set to "high confidence" (0.700).

SDS-PAGE and Western Blots—Equal total protein amounts (Nanoquant Assay, Roth) from membrane-enriched and soluble retinal fractions were separated by SDS-PAGE (12% gels) and either stained with Coomassie Brilliant Blue or blotted onto PVDF membranes. After blocking for 1 h in 5% BSA, blots were incubated with antibodies against TIM23 (1:2500, BD Transduction Laboratories) or glutamine synthetase (GS, 1:1000, BD Transduction Laboratories) at 4 °C overnight. Binding was detected by appropriate HRP-coupled secondary antibody incubation (2 h at RT) and signal development with ECL (GE Healthcare) followed by film exposure.

Immunohistochemistry-Enucleated eyes were punctured in the anterior part and immersion-fixed with Bouin's solution (Sigma). After fixation, eyes were dehydrated in a series of alcohols. Posterior parts of fixed eyes were then cut into four quadrants as described earlier(16) and resulting specimens were embedded in paraffin. Tissue sections (from the nasoventral quadrant) were cut (5  $\mu$ m) and mounted on coated slides (Super Frost Plus; Microm), deparaffinized, and rehydrated. Heat antigen retrieval was performed at 99 °C for 15 min in 0.1 M EDTA-NaOH buffer pH 8.8 (17). We used polyclonal rabbit antibody specific for caveolin 1 (CAV1; Santa Cruz sc-894, 1:50), phosphofocal adhesion kinase (pFAK, Cell Signaling, 1:50) and integrin alpha 1 (CD49a, Lifespan Biosciences, 1:50) for candidate detection in tissues. For fluorescence labeling, secondary anti-rabbit IgG antibody coupled to alexa568 or alexa488 (both Invitrogen, 1:500) or anti-rabbit IgG Biotin (Linaris) 1:2000 followed by incubation with streptavidin-Cy5 (Linaris 1:500) were used for signal detection. Triple labelings were performed consecutively, with blocking steps (Protein-Block, Dako) between single antibody incubations. For conventional staining, CAV1 signal was detected with secondary antibody antirabbit IgG biotin (Linaris, 1:1000), followed by incubation with peroxidase-conjugated streptavidin (Vectastain ABCElite:HRP kit; Linaris). Binding was visualized with the Vector HRP substrate kit VIP, which results in violet color (Linaris). Fluorescence stainings were photographed with an Axio Imager M1 (Zeiss), visualized with the Axio Vision 4.6.3 software (Zeiss), and processed with Photoshop CS3. VIP color stainings were scanned and further processed with image analysis software (see below).

Image Analysis—All VIP-stained slides were scanned at 20× objective magnification by a Mirax Scanner (Zeiss). For each of the resulting digital slides, subsets (regions of interest) were defined from areas of retina from the median to central areas (16) and analyzed using commercially available software (Definiens Enterprise Image Intelligence™ Suite, Definiens) (18, 19). A rule set was developed to detect and quantify semantic classes. In a first step, the algorithm segments pictures iteratively, recognizing groups of pixels as objects.



TABLE I

b value	a value	Pathway	Source	Size	Overlap downregulated in ERU <sup>1</sup>	Overlap unchanged <sup>2</sup> or upregulated <sup>3§</sup>
	- 0					)
0.000	0.000	Akap95 role in mitosis and chromosome dynamics	BioCarta	<u>က</u>	DDX5*; H3F3A	
0.000	0.000	Citrulline biosynthesis	HumanCyc	6	GLS; PRODH*	
0.000	0.000	Amino acid transport across the plasma membrane	Reactome	29	SLC38A3; SLC3A2	
0.000	0.000	RNA polymerase I Promoter clearance (includes "RNA Polymerase I promoter opening")	Reactome	54	H3F3A; HIST1H2BJ; HIST1H4K	
0.000	0.000	Notch signaling pathway	KEGG	47	CTBP2; KAT2A*	
0.000	0.005	Cardiac muscle contraction	KEGG	79	ATP1A3; ATP1B1; COX411; COX5B; COX6B1; COX7A1; COX7A2; COX7A2L*; MYH6; MYH7*; UQCR*; UQC7B	ATP1A1; ATP1B2; ATP2A2; COX5A; CYC1;TPM2; UQCRC1; UQCRC2; UQCRH;
0.001	0.013	Visual signal transduction	BioCarta	4	GNAT1; GRK1*; SLC25A18*; SLC25A22*	GNB1
0.001	0.012	Visual signal transduction: Rods	PID	25	GNAT1; GRK1*; RDH12; SAG	GNB1
0.004	0.044	Visual signal transduction: Cones	PID	24	ARR3*; GRK1*; RDH12	GNB1
0.004	0.037	Transcription (includes "RNA polymerase I transcription")	Reactome	175	H3F3A; HIST1H2BJ; HIST1H4K	PTRF <sup>§</sup> *
0.004	0.025	Formation and maturation of mRNA transcript (includes "elongation and processing of capped transcripts"; "mRNA splicing"; "wiral messenger RNA synthesis"; "processing of capped intron-containing pre-mRNA")	Reactome	167	HNRNPC*; HNRNPK; HNRNPM*; PCBP1; PCBP2	HNRPU*; HNRPR*; HNRPD*
0.009	0.057	Electron transport chain	Reactome	76	COX41; COX5B; COX6B1; COX7A2L*; NDUFA4*; NDUFA9; NDUFB1*, NDUFB10; NDUFB1†; NDUFB4; NDUFB5*; NDUFB8*; NDUFS2; UQCR*; UQCRB	CYCS*; CYC1; COX5A; ETFB*; NDUFS1; NDUFS3; NDUFS5*; NDUFS7; NDUFAB1*; NDUFA6*; NDUFS8; NDUFA13; NDUFV1*; NDUFV2*; NDUFB9*; NDUFA10; SDHC; UQCRC1; UQCRC2; UQCRH;

 $^1$   $\rho<0.05$  and more than 2-fold upregulated.  $^2$   $\rho>0.05$  or less than 2-fold upregulated.  $^3$   $\rho<0.05$  and more than 0.5-fold downregulated in ERU.  $^*$  Identified and quantified by only one peptide.

MOLECULAR & CELLULAR PROTEOMICS

Pathway enrichment analysis with proteins uprequlated in ERU

p value	q-value	Pathway name	Source	Size	Overlap upregulated in ERU <sup>1</sup>	Overlap unchanged <sup>2</sup> or downregulated <sup>3§</sup>
0.00	0.00	B cell survival pathway	BioCarta	50	ITGA1*: ITGB1	
		Action proposed to a contraction	o tro		DOM*: LI A A: TABA: TABA	
0.000	0.000	Annigen processing and presentation	בו הי הי	- (	DZINI, FICA-A, IAFI, IAFZ	
0.000	0.000	IL2	NetPath	65	ICAM1; STA11	
0.000	0.000	Erk and pi-3 kinase are necessary for collagen binding in corneal epithelia	BioCarta	34	ACTA1*; ACTN1*; ACTN4; GSN; ITGA1*; ITGB1; PFN1*	
0.000	0.000	ABC-family proteins mediated transport	Reactome	4	ABCD3*; APOA1	
0.000	0.000	Extrinsic prothrombin activation pathway	BioCarta	18	F3*; FGA; FGB; FGG	
0.000	0.000	HDL-mediated lipid transport	Reactome	Ξ	ALB; APOA1	
0.000	0.000	TNF receptor signaling pathway	PID	47	CAV1; STAT1	
0.000	0.000	Primary immunodeficiency	KEGG	35	TAP1; TAP2	
0.000	0.000	Autoimmune thyroid disease (contains "Allograft rejection"; "Graft-versus-host disease")	KEGG	25	HLA-A; HLA-C	
0.000	0.000	Immunoregulatory interactions between a Lymphoid and a non-Lymphoid cell	Reactome	152	B2M*; CXADR; HLA-A; HLA-C; ICAM1; ITGB1	C3; CD81
0.000	0.002	Integrin cell surface interactions (includes "Integrin alphallbbeta3 signaling"; "Grb2:SOS provides linkage to MAPK signaling for Intergrins")	Reactome	8	FGA; FGB; FGG; FN1; ICAM1; ITGA1*; ITGAD*; ITGAV; ITGB1; ITGB8*; LAMB2; LAMC1; VTN*	RAP1B; BSG; COL4A5*; ITGAD*; LAMA5; CO2A1
0.000	0.003	Integrin signaling pathway	BioCarta	36	ACTA1*; ACTN1*; ACTN4; CAV1; ITGA1*; ITGB1	HRAS*
0.003	0.024	Formation of Fibrin Clot (Clotting Cascade)	Reactome	33	F3*; FGA; FGB; FGG	C1QBP
0.003	0.023	Lipoprotein metabolism	Reactome	27	ALB; APOA1; HSPG2; P4HB	SAR1B <sup>§</sup> *
0.003	0.022	Complement and coagulation cascades	KEGG	69	F3*; FGA; FGB; FGG	C3
0.005	0.030	ECM-receptor interaction	KEGG	84	CD44: COL6A1*; FN1; HSPG2; ITGA1*; ITGAV; ITGB1; ITGB8*; LAMB2; LAMC1; VTN*	CD47*; CO2A1; DAG1*; ITGAD*; LAMA5; SV2A; SV2B <sup>§</sup> ; TNXB
0.005	0.033	Ucalpain and friends in cell spread	BioCarta	56	ACTA1*; ACTN1*; ACTN4; ITGA1*; ITGB1	RAC1; SPTAN1
0.010	0.059	Formation of Platelet plug (includes "Platelet activation", "Platelet Aggregation (Plugg Formation)", "pl 30Cas linkage to MAPK signaling for integrins"; "Response to elevated platelet cytosolic Ca <sup>2++</sup> , "Platelet edgeranulation" and "Exocytosis of Alpha granulation" and "Exocytosis of Alpha granulation".	Reactome	135	ACTN1*; ACTN4; ALB; ALDOA; CD9; CLU; FGA; FGB; FGG; FN1; GNG2*; ITGB1; LAMP2*	GNB1; GNB2; GNB3; GNB4*; GNG7; GNG12*; GNA0; GNA13; ITGAD*; RAP1B; GNG48*; GNG108*
0.010	0.057	Focal adhesion	KEGG	202	ACTN1*; ACTN4; CAV1; COL6A1*; FLNA; FN1; ITGA1*; ITGAV; ITGB1; ITGB8*; LAMB2; LAMC1; VTN*	ACTB; CDC42; COL2A1; CTNNB1; HRAS; ITGAD*; LAMA5; MYLK2*; PPP1CA*; RAC1; RAP1B; TNXB

 $<sup>^{1}</sup>p<0.05$  and more than 2 fold upregulated.  $^{2}p>0.05$  or less than 2 fold upregulated.  $^{3}p<0.05$  and more than 0.5 fold downregulated in ERU.  $^{*}$  Identified and quantified by only one peptide.

Further in the process, the objects are classified based on staining intensity, morphology, neighborhood, and special color features and graded "VIP-area" as light red, dark red, and black red. The relative areas of the specific VIP stained areas were calculated in comparison to the total tissue area. Statistical analysis was performed by Mann-Whitney test. Significance level was defined as \*\*\*\*  $p \leq 0.001$ .

#### **RESULTS**

We first explored whether it is feasible to generate membrane-enriched fractions from individual specimen of horse retina in sufficient quality and quantity to perform a label-free proteomic comparison. To this end, we applied and adapted a previously published method (9) which was designed for membrane enrichment from small tissue samples (for analytical strategy applied here, see Fig. 1A). Because horse retina specimen weigh on average around 200 mg, it was possible to qualitatively assess membrane enrichment with SDS-PAGE and subsequent Coomassie Blue staining of the gels. Equal total protein amounts from membrane-enriched fraction and pooled soluble fractions collected during the extraction steps were loaded and qualitative comparison of the gel images demonstrated a very different appearance of band patterns between membrane-enriched fraction and soluble fraction (Fig. 1B). When soluble and membrane-enriched fractions were probed with antibodies against mitochondrial import inner membrane translocase subunit Tim23 (TIM23) as a marker for membrane proteins and with anti-glutamine synthetase (GS) antibodies as a marker for soluble proteins, Western blot analysis reveals very high enrichment for the respective compartments (Fig. 1B). TIM23 is exclusively detected the membrane-enriched fraction and the majority of GS is detected in the soluble fraction. This suggests that enrichment strategy is sufficient for generating crude membrane fractions. In line with these qualitative data, we found that a major proportion (57%) of proteins identified were annotated to the GO term "membrane" (Fig. 1C) and prediction of transmembrane domains by TMHMM resulted in 297 proteins with one or more transmembrane domains (TMD) predicted. Among them were FAM38A (1 peptide, Mascot score 81) with 23 predicted TMDs, SLC7A4 (1 peptide, mascot score 33) with 14 predicted TMDs, 9 proteins with 12 predicted TMDs (GLUT1, SLC4A1, SLC6A1, SLC6A9, SV2A, SLC16A3, SV2B, NNT, STT3A), 6 proteins with 11 predicted TMDs (SLC4A7, SLC12A7, ABCA4, SLC4A10, SLC15A2, SLC16A1), 9 proteins with 10 predicted TMDs (SLC37A4, SLC6A11, STT3B, SLC38A3, SEC61A1, SLC1A3, ATP8B1, SLC2A3, ATP1A1), 5 proteins with 9 predicted TMDs (ATP2A2, SLC1A4, SLC1A5, SLC1A2, SLC32A1), 8 proteins with 8 predicted TMDs (NIPAL4, SLC17A7, CEPT1, COX15, PTDSS1, DHCR7, PMCA, ATP1A3), 8 proteins with 7 TMDs, 9 proteins with 6 TMDs, 16 proteins with 5 TMDs, 17 proteins with 4 TMDs, 30 proteins with 3 TMDs, 27 proteins with 2 TMDs, and 151 proteins with 1 predicted TMD (see supplemental Table 1 for all details). Among the proteins annotated to the GO term "membrane" (508 proteins), 45.9%

qualified for GO term "plasma membrane", 22% for GO "mitochondrial envelope", 16.1% "endoplasmic reticulum membrane", 15.2% "vesicle" and 3.1% "nuclear membrane" (Fig. 1*D*).

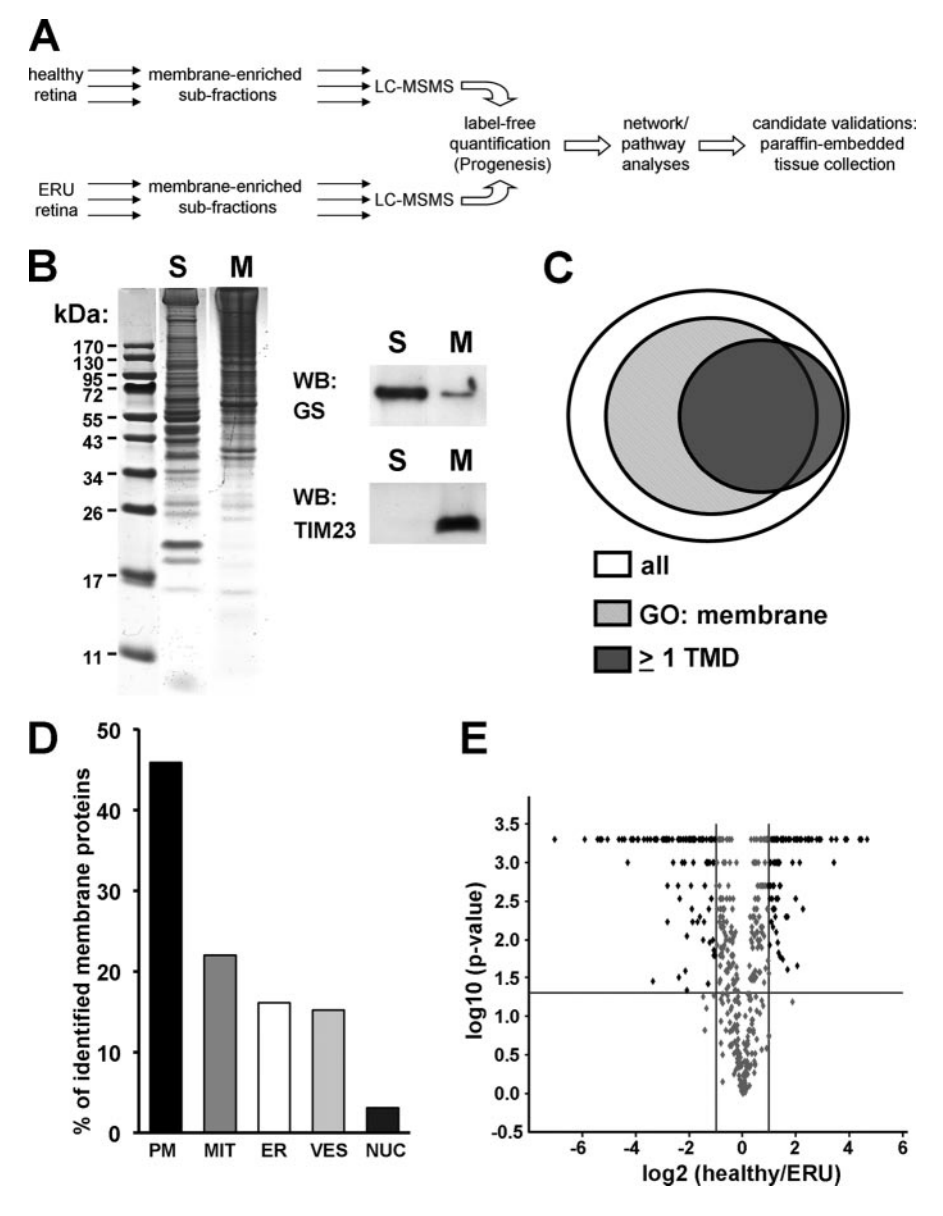
To assess technical reproducibility of the whole process (tissue fractionation, in solution tryptic digestions, and nano-LC-MS/MS (overview in Fig. 1A)), we performed membrane enrichment and subsequent mass spectrometric analysis on retinal tissue divided into three equal parts (40 mg each) for one healthy and one ERU specimen. After the complete workflow of label-free quantification, we assessed the variation between cumulative peptide intensities for each identified protein for those replicate measurements (all details given in supplemental Table 1). The average coefficient of variation was 24.1% for all identified proteins in healthy and 17.1% in ERU tissue if proteins that were also identified with only one peptide were considered. Variation was even lower when only proteins identified with two or more peptides were considered: 17.1% (healthy) and 11.2% (ERU). The reproducibility of protein identifications was high, with 885 proteins identified in all three replicates (99.1% of all protein identifications) of healthy and 887 (99.3%) of ERU tissue.

Quantitative Comparisons of Membrane-Enriched Tissue Fractions Yields 179 Differentially Detected Candidate Proteins - After having assessed the applicability of membraneenrichment to retinal specimen, we performed such enrichment on one healthy and one ERU retina. Because such samples are scarce, we took advantage of the fact that we could perform membrane enrichment with as little as 40 mg of tissue and accordingly divided the specimen into three such parts. This generated three technical replicates which allowed us to perform statistics on technical variation within the experiment. We processed those samples for mass spectrometry, performed LC-MSMS as described in the experimental procedures, and performed quantitative analysis with the Progenesis software package. Briefly, all detected features in the 2D maps were aligned between samples, normalized, and assigned to either the healthy or the ERU group. Then, ANOVA was performed on all normalized peptide intensities. All features with MS/MS data were then subject to identification with Mascot against the Ensembl horse protein database and search results were implemented into the experiment file. Peptide identifications were then merged into nonredundant protein identifications.

As a result we could identify a total of 893 proteins, among them 481 with  $\geq 2$  peptides (Fig. 1*E*). 334 proteins (179 with  $\geq$  2 peptides) were found differentially expressed between healthy and ERU (*p* < 0.05 and more than 2-fold regulated). 172 proteins (96 with  $\geq$  2 peptides) of these were upregulated in ERU (see supplemental Table 2), 162 proteins (83 with  $\geq$  2 peptides) were downregulated in ERU (see supplemental Table 3).

Network and Pathway Enrichment Analysis for the Differentially Expressed Proteins—The complete list of identified pro-

Fig. 1. A, workflow overview: membrane proteins were enriched from retina specimen (healthy and ERU) followed by tryptic digests and mass spectrometric measurements (Orbitrap). Raw files were loaded into Progenesis software for quantitative label-free analyses. Peptides were detected and aligned across samples and grouped into either healthy or ERU group. Quantification was performed on the peptide level by accumulating intensities of extracting ion current (XIC) for all isotopes over the retention time of a given peptide and comparison of the resulting peak volumes between groups (ANOVA). After identification of peptides with Mascot in Ensembl horse database. identified peptides were merged into proteins and significantly regulated proteins were subjected to GO analyses, protein network analyses (STRING) and pathway overrepresentation analyses. Selected candidate markers for ERU were validated on large sample sizes by immunohistochemistry on paraffin-embedded tissue specimen and image analyses. B, equal total proteins amounts of membrane-enriched fraction (M) and soluble fraction (S) extracted from horse retina were separated by SDS-PAGE and either stained with coomassie or blotted and probed with antibodies against mitochondrial import inner membrane translocase subunit Tim23 (TIM23) or glutamine synthetase (GS). Coomassie staining reveals distinct band pattern for membrane-enriched fraction as compared with soluble fraction. GS, a cytosolic protein is strongly enriched in the soluble fraction and only traces are still remaining in the membrane-enriched fraction. TIM23, a protein expressed in mitochondria inner membrane is only detected in the membrane-enriched fraction. C, proportion of membrane protein is the membrane-enriched fraction. All identified proteins (white area) were subject to GO analyses with respect to subcellular localization and to prediction of transmembrane domains with TMHMM. 508 proteins were found to be included in the GO



term "membrane" (gray area) and 297 had 1 or more predicted transmembrane domains (blue area). D, Subcellular localization of identified membrane proteins according to GO: PM - plasma membrane; MIT - mitochondrial envelope; ER - endoplasmic reticulum membrane; VES - vesicle; NUC - nuclear membrane. E, Volcano plot showing differentially abundant proteins (log2 fold change, x axis; log10 p value ANOVA, y axis) from healthy against ERU membrane-enriched tissue fractions quantified with two or more peptides. Horizontal line indicates p=0.05 and vertical lines indicate 2 fold and 0.5 fold abundance changes. p values of 0.000 were set to 0.0005 in order to limit scaling. Black diamonds indicate regulated proteins, gray diamonds indicate unregulated proteins.

teins was transformed to a nonredundant gene identifier list of the respective human homologues and then subjected to pathway enrichment analysis by ConsensusPathDB as well as used for analyzing protein networks by STRING version 8.2. To detect pathways or networks either upregulated or downregulated during uveitis, the candidate protein list was split into the respective parts (see supplemental Tables 2 and 3).

STRING analyses with the subsets of either upregulated or downregulated proteins in ERU resulted in a loose network for the downregulated proteins (supplemental Fig. 1), which contains two clusters of higher connectivity around mitochondrial proteins and proteins involved in visual processes. However, the network produced by STRING for the subset of upregulated proteins (Fig. 2A) contains a highly connected subnetwork which contains several membrane or membrane-associated proteins (Fig. 2B), such as PELO (ITGA1, Integrin alpha-1 precursor = CD49a antigen), CAV1 (Caveolin 1), ITGAV (Integrin alpha-V precursor = CD51 antigen), ITGB1 (Integrin beta-1 precursor = CD29 antigen), ICAM1 (Intercellular adhesion molecule 1 precursor = CD54 antigen), VTN

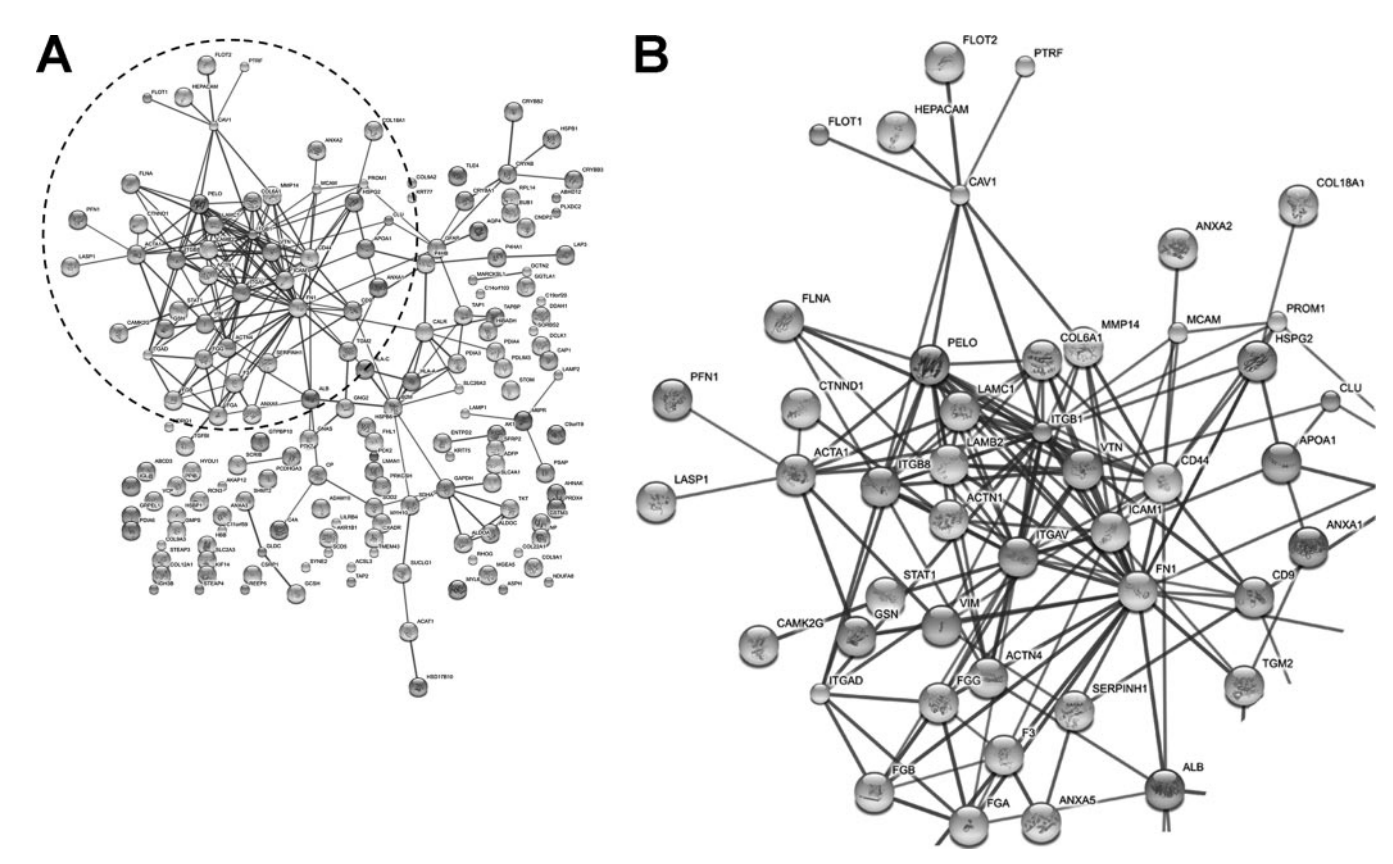


Fig. 2. Protein-protein interaction (PPI) map of up-regulated proteins in ERU (p < 0.05 and more than 2 fold up-regulated). A, Total cluster built with STRING allowing for experimentally verified and predicted PPIs at high confidence level (0.700). One highly connected subnetwork was evident which is enlarged in B.

(Vitronectin), FN1 (Fibronectin), CD44, MMP14 (Matrix metalloproteinase-14), ITGB8 (Integrin beta-8 precursor), LAMC1 (Laminin subunit gamma-1 precursor), and LAMB2 (Laminin subunit beta-2 precursor). STRING analysis with the subset of unregulated proteins (supplemental Table 4) resulted in an overall loosely connected network which also comprised two highly connected subnetworks, one involving mitochondrial membrane respiratory chain NADH dehydrogenase (complex I) components and another with ribosomal proteins (supplemental Fig. 2). This confirms stable expression of biosynthesis and energy metabolism related house keeping proteins.

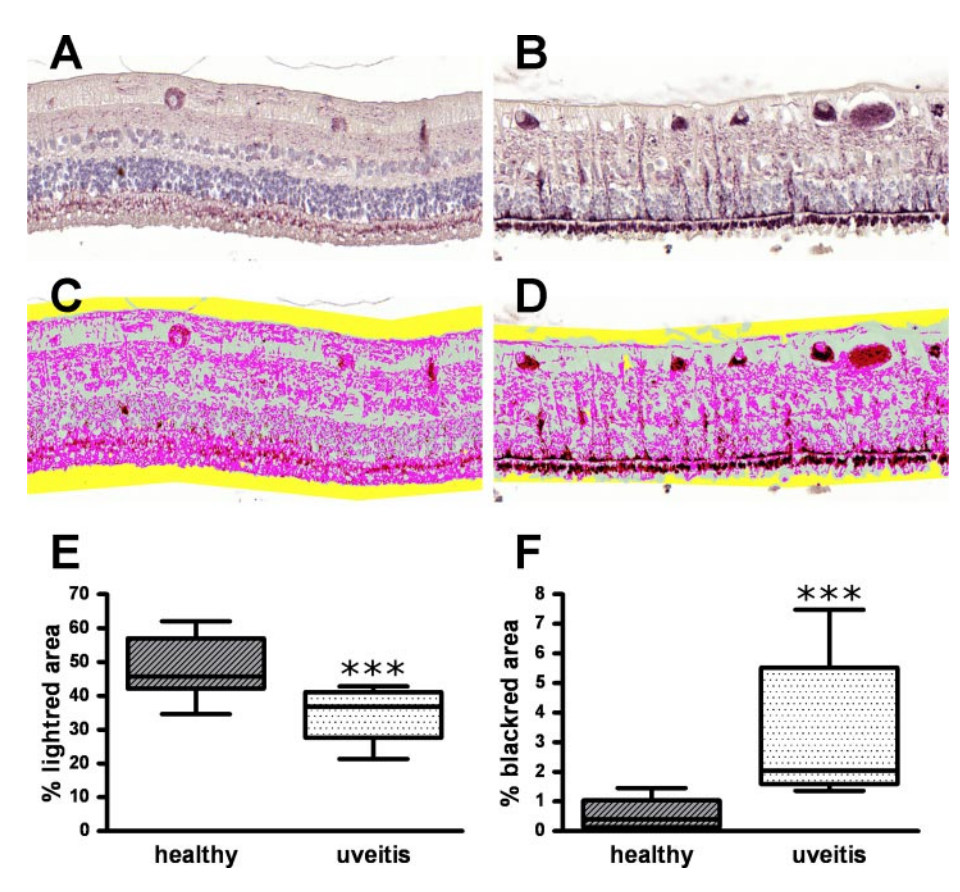
Pathway enrichment analysis with the ConsensusPathDB database yielded several significantly ( $p \leq 0.01$ ) downregulated pathways in ERU (see Table I), among them are rod and cone "visual signal transduction" (PID, BioCarta), reflecting the ongoing retinal tissue destruction in uveitis. The significantly upregulated pathways in ERU (see Table II) contain "antigen processing and presentation" (BioCarta), "B cell survival pathway" (BioCarta), "exocytosis of alpha granule" (Reactome), "IL2" (NetPath), "TNF receptor signaling pathway" (PID), "immunoregulatory interactions between a lymphoid and a nonlymphoid cell" (Reactome), "integrin cell surface interactions" (Reactome), "integrin signaling pathway" (Bio-

carta), "ECM-receptor interaction" (KEGG), and "focal adhesion" (KEGG). Within the focal adhesion pathway, a total of 13 proteins (ACTN1; ACTN4; CAV1; COL6A1; FLNA; FN1; ITGA1; ITGAV; ITGB1; ITGB8; LAMB2; LAMC1; VTN) have been found upregulated in ERU and 12 additional proteins from this pathway were unchanged based on the criteria p < 0.05 and healthy/ERU < 0.5-fold regulation (see supplemental Fig. 3; KEGG pathway "focal adhesion with color-coded regulation factors").

Candidate Validation by Immunohistochemistry on Tissue Collections/Repositories—After identification of regulated proteins and their allocation to functional pathways, the significance of these results remained to be validated. Because fresh tissue samples of ERU and healthy horses are rare, we chose to validate the findings on the existing large tissue repository which has been collected over some years from both ERU cases as well as non-eye-diseased control horses. Within the tissue collection, we cover all different stages of tissue destruction occurring in ERU pathology as well as individual differences reflecting the outbred horse population.

We selected caveolin1 (CAV1) as candidate membrane protein to be validated because it was listed in several of the upregulated pathways, such as "TNF receptor signaling path-

Fig. 3. Candidate validation immunohistochemistry and image analysis. Retinal specimen from healthy (A, C) and ERU cases (B, D) were stained with antibodies against caveolin-1 (CAV1) and staining was developed with VIP (purple color). Stained sections were scanned and processed with a pre-developed rule set for image analysis (C, D). VIP staining intensities were graded into "lightred" (pink areas in C and D), "darkred" (red areas) and "blackred" (black areas) and respective areas were compared with total tissue areas (containing also unstained areas; gray in C and D). Percent "lightred area" significantly (p = 0.0007) decreases in ERU (E), whereas "darkred" (data not shown) and "blackred" (F) areas increase in ERU (F, p < 0.0001 for "blackred areas"). Quantitative analyses were performed on 10 healthy and 10 ERU cases and significance was calculated with the Mann-Whitney test.



way" (PID), "integrin signaling pathway" (BioCarta) and "focal adhesion" (KEGG). CAV1 was identified in the proteomics comparison with two peptides (total mascot score: 127) and an upregulation of 16-fold in ERU as compared with the healthy control.

Immunohistochemistry on 10 healthy and 10 ERU tissue samples confirmed upregulation in ERU. Although the appearance of the tissues is heterogeneous for the ERU cases, reflecting different stages of disease and disease-related tissue destruction as well as potential differences between individuals, the upregulation of CAV1 in ERU is consistent (Fig. 3). To quantitatively assess CAV1 expression, we performed an automated staining routine with a stable chromophore that accumulates over time in direct correlation to CAV1 level as detected by the primary antibody. Image analysis with an algorithm detecting different gradings of staining intensities enabled us to automatically detect the respective areas and relate them to total tissue areas. As shown in Figure 3, the relative amount of areas containing most intense (black-red) staining are significantly upregulated in ERU (\*\*\*, p < 0.0001; Mann-Whitney test) and, concomitantly, areas containing lowlevel intensities (light red) for CAV1 are significantly downregulated (\*\*\*, p = 0.0007) in ERU.

Most interestingly, the staining intensity, respective CAV1 upregulation, is very pronounced at the level of the OLM (Fig. 3, B and D), a structure where photoreceptors and retinal Mueller glial cells build a tight border against adjacent extra-

cellular space by accumulation of tight junctions. Upregulation of CAV1 in this area suggests that this structure might undergo changes in ERU.

Because "focal adhesion" was one of the significantly upregulated pathways from the Consensus PathDB analysis and CAV1 is part of this pathway (see supplemental Fig. 3), we further investigated whether we could find evidences for increased focal adhesion signaling in ERU tissue, especially at the level of the OLM. Immunofluorescence triple-labeling demonstrated regulation of pFAK together with CAV1 and integrin alpha 1 (ITGA1), which was also among the upregulated proteins identified in the proteomics screen (one peptide, mascot score 60, upregulated 3-fold in ERU) and is a direct neighbor to CAV1 in the focal adhesion KEGG pathway (see supplemental Fig. 3). The triple-labeling (n = 4) confirms upregulation of integrin alpha 1 (ITGA1) in ERU (4), which in healthy retina is exclusively expressed at the level of photoreceptor segments, whereas in ERU becomes upregulated throughout the tissue as well as at the level of the OLM (arrow). This staining partly overlaps with pFAK which also increases in ERU as compared with healthy controls especially at the OLM and throughout the retina. Both, pFAK and ITGA1 staining in ERU overlaps with CAV1 throughout the tissue as well as at the OLM, suggesting as yet undescribed active processes related to focal adhesion pathway in ERU (Fig. 4).

## DISCUSSION

LC-MS/MS Workflow for Protein Identification From Membrane-Enriched Retinal Fractions-The present study aimed at identifying changes in membrane protein expression related to spontaneous autoimmune uveitis. Since we have studied protein expression in retina of ERU cases before using conventional 2D gel-based proteomics, we know that this disease presents with activation of retinal Müller glial cells and with a break-down of the blood-retinal barrier (BRB) with variable severity (5). The latter poses serious problems with respect to identifying tissue-related protein expression changes as there is massive influx of serum-derived proteins which creates a strong bias for serum-derived proteins. Additionally, because autoimmune uveitis involves autoagressive T cells entering and attacking the retinal structures, this process is likely to be triggered by changes on the cellular and tissue surfaces. Therefore, we decided to enrich retinal specimen for their membrane proteins and focus the differential analyses on this tissue fraction. To this end, we adapted a previously reported method (9) which was established for membrane enrichment from little tissue sample material. In contrast to the previously reported method, however, we did not resolve the membrane-enriched fraction in detergents but directly subjected the membrane proteins to tryptic digestion in the presence of the surfactant RapiGest™. This resulted in a reproducible workflow which led to overall identification of 57% membrane proteins (based on GO annotation term "membrane") from the enriched fractions. This is comparable to the previously published method in which approximately 65% of the membrane proteins were identified (9). The advantage is that the adapted method is easier because it requires no additional desalting column for detergent removal and can thus be expected to be more reproducible. In accordance with this, we found the overall variability percent coefficient of variation (CV) to be between 11 and 17% based on robustly identified proteins (≥ 2 peptides). Since the technical variability was not investigated in the publication of the original protocol, (9) we cannot directly compare our findings with these experiments. Therefore, we compared our variability to a recently published study also involving enrichment strategies in which a of as high as 30% is discussed as reproducible (20), so the variability of the adapted method applied here is low.

Membrane enrichment resulted in identification of 57% proteins from GO category "membrane" which is consistent with the proportion achieved by the previously published (9) method. Because the GO term "membrane" also includes membrane-associated proteins, we additionally predict potential TMDs for all identified proteins. As a result, 297 proteins were predicted with 1 or more TMDs, which represent a proportion of 33.3%. Interestingly, the group of proteins with predicted TMD does not completely overlap with those proteins sub-summarized under the GO term "membrane" (see Fig. 1*D*), and several proteins (27) which have a predicted

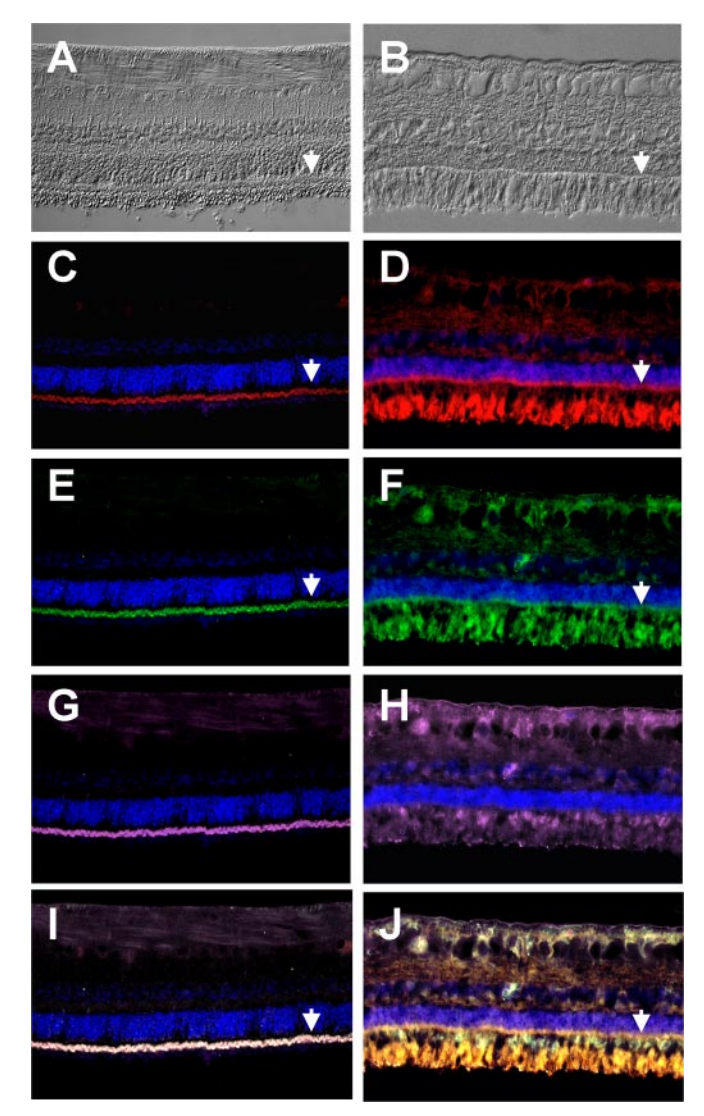


FIG. 4. Triple labeling of retinal sections from healthy (A, C, E, G, I) and ERU cases (B, D, F, H, J) with antibodies against integrin alpha 1 (ITGA1, green, C and D) and phospho-focal adhesion kinase (pFAK, red, E and F) and caveolin 1 (CAV1, purple, G and H). In ERU cases a pronounced increase of both ITGA1 and pFAK is observed throughout the tissue and at the level of the outer limiting membrane (OLM, arrowheads). There is considerable co-localization of pFAK, ITGA1 and CAV1 immunostaining indicated in the overlay images (I and J, triple staining in white color), throughout the tissue as well as at the level of the OLM. Representative images from four healthy and four ERU cases are shown.

TMD are not among the membrane-annotated ones (see all details in supplemental Table 1). Among them are transmembrane protein 221 (TMEM221) which has two predicted TMDs and synaptic glycoprotein SC2 (TECR) with three predicted TMDs. Uniprot entries of the respective human orthologues suggest four and three transmembrane domains, respectively, and because GO classification is based on the human orthologues, the GO annotation is in these cases incomplete. Both proteins have, to the best of our knowledge, not yet been detected in retinal tissue.

Identification of proteins relies on the completeness of the sequence data for a given species. Because the results from a new whole genome sequencing initiative were published for the horse genome recently (21), we could significantly increase the total identification rate from formerly 383 equine proteins (National Center for Biotechnology Information database, data not shown) to a total of 893 nonredundant protein identifications from horse by using the respective release (Ensembl). Among these are many retina-specific proteins, such as retina-specific adenosine triphosphate-binding cassette transporter (ABCA4), cone-arrestin (ARR3), transducin alpha-1 (GNAT1), rhodopsin kinase (GRK1), phosducin (PDC), peripherin-2 (PRPH2), retinol-binding protein I (RBP1), interphotoreceptor retinoid-binding protein (IRBP), retinol dehydrogenase 12 (RDH12), RPE-retinal G protein-coupled receptor (RGR), cellular retinaldehyde-binding protein (CRALBP), rod outer segment membrane protein 1 (ROM1), retinoschisin (RS1), and S-antigen (SAG). However, the visual pigment rhodopsin which is a major part of the membrane fraction of photoreceptors was not among the identified proteins. The reason for not identifying this protein, however, is likely the incompleteness of the horse genome. Visual pigment rhodopsin was not yet included in this database, and can thus not be identified. In an unrelated study where we applied the membrane enrichment to mouse retina, we could readily identify rhodopsin (unpublished data) from the ensemble mouse database.

Taken together, we conclude that the presented method is suitable to compare membrane-protein enriched fractions from retinas and results in a much increased analysis depth compared with conventional 2D gel-based proteomics comparisons (5, 22).

Correlation to Previous Proteomics Studies in ERU-When comparing the identified proteins and their respective expression level between healthy and ERU specimen, we found a balanced proportion between upregulated and downregulated proteins in the disease and many proteins unchanged in expression. Additionally, we had none of the previously identified highly abundant serum proteins (5) present in the ERU tissue membrane fractions except for albumin (ALB) and apolipoprotein A-I (APOA1). This confirms that our approach to enrich for membrane proteins depletes the BRB-derived serum proteins and thus increases the sensitivity of the comparative analysis. In line with our previous proteomics comparisons (5), we found an increase of glial fibrillary acidic protein (GFAP) and vimentin (VIM) and a decrease of glutamine synthetase (GLUL) corroborating the involvement of retinal Müller glial cells in disease pathology. Additionally, we found a decrease of the inwardly rectifying potassium channel Kir4.1 (KCNJ10) which is well-known to be downregulated in response to retinal pathologies such as retinal detachment (23), retinal ischemia (24), and ocular inflammation (25), likely resulting in glial swelling.

Expression Changes Related to ERU Pathology—Pathway enrichment analyses enabled us to group the observed ex-

pression changes between healthy and ERU specimens. Among the significantly downregulated pathways were "visual signal transduction" pathways from rods and cones. This is an expected result and confirms previously reported findings that normal retinal structure and function is severely impaired in autoimmune uveitis finally leading to complete blindness in the end stage of the disease (3). Other downregulated pathways include "akap95 role in mitosis and chromosome dynamics," "citrulline biosynthesis," "amino acid transport across the plasma membrane," and "notch signaling pathway" all represented with only two overlap members identified from our screen. Although this results in significant enrichment, the relevance for the disease remains to be elucidated. The pathways "cardiac muscle contraction", "cormation and maturation of mRNA transcript," "transcription," and "electron transport chain" present with larger numbers of overlapping proteins; however, many of the pathway-related proteins identified here are not downregulated (see last column in Table I) but stably expressed. In particular, the "electron transport chain" pathway, representing mitochondrial energy production pathway, has both downregulated members as well as unregulated members. Energy balance may be critical for disease progression since it has been shown that during retinal degenerations induced by mutations, energy deprivation is a major trigger of cell death (26). Thus, the tendency of loss of energy-supplying processes may be indicative for misbalance in energy supply and consequent neuronal degeneration; however, since many pathway members are still unchanged, this process might be in an early phase.

In contrast to pathways and processes downregulated in ERU which may mostly reflect loss of retina-specific neurons and functionalities, pathways upregulated in ERU may be potentially indicative for the cellular mechanisms related to disease progression. Among the most highly upregulated proteins in ERU are antigen peptide transporter 2 (TAP2) and antigen peptide transporter 1 (TAP1), which together form the so-called TAP complex as well as tapasin isoform 1 (TAPBP), beta-2-microglobulin (B2M), protein disulfide-isomerase A3 (PDIA3), calreticulin (CALR) and major histocompatibility complex (MHC) class I, which are associated with the TAP complex and together form the so-called peptide-loading complex located at the endoplasmic reticulum membrane (27). This is reflected by the pathway "antigen processing and presentation" being among the significantly enriched pathways derived from the subset of upregulated proteins (Table II). The peptide-loading complex is transporting peptides from the cytosol into the lumen of the endoplasmic reticulum and loading them onto MHC class I molecules for cell surface presentation. With few exceptions, most cell types constitutively express the peptide-loading complex molecules; however, IFN $\gamma$  and TNF $\alpha$  have been shown to induce the expression of both MHC class I as well as TAP1 and TAP2 (28, 29). Since we have reported earlier a marked upregulation of IFN $\gamma$ in ERU (5), the upregulation of peptide-loading complex components reported here may be a consequence of IFN $\gamma$  induction. Future studies will aim at investigating whether in ERU levels of peptide-loading complex correlate with IFN $\gamma$  levels. Currently these analyses are not feasible because appropriate antibodies against equine components of the TAP complex are not available.

Other significantly enriched pathways include "TNF receptor signaling pathway," "integrin signaling pathway," and "focal adhesions." Interestingly, CAV1 participates in all three pathways and we thus decided to select CAV1 for a larger scale histological validation screen. CAV1 is a membrane protein with two TMDs and was identified and quantified based on two peptides (total mascot score 127) as being upregulated in ERU 16-fold (healthy/ERU = 0.06). When we quantified the intensities of the staining signals produced with an anti-CAV1 antibody, we could confirm the initially reported upregulation. CAV1 expression is significantly increased in ERU and, although retinal tissue specimens are variable with respect to ERU-related destruction both within one specimen as well as between specimens, the increase of CAV1 expression is consistent. Histologically, increased CAV1 expression was observed along photoreceptor segments as well as along vertical structures throughout the retina resembling Müller cell processes and in retinal ganglion cells. However, the most pronounced increase of CAV1 expression was observed at the level of the OLM, which is a tight border that separates the retina from the adjacent extracellular space (interphotoreceptor matrix) and is formed by tight junctions between retinal Müller cells and photoreceptors (30). This finding, together with the significantly upregulated pathway "focal adhesions," prompted us to investigate further whether changes of additional proteins from this pathway would also be apparent in the OLM. We selected ITGA1, which was identified as being upregulated in ERU (3-fold)(only based on one peptide (Mascot score 60)) and which was also included as a direct neighbor in the STRING network for upregulated proteins (Fig. 2, PELO). Additionally we aimed at challenging the predictions resulting from pathway enrichment analyses and probed for the phosphorylated form of pFAK which was not among our identified proteins, but is the first downstream kinase involved in focal adhesion signaling as suggested by the KEGG pathway model (see supplemental Fig. 2). The triple labeling on ERU tissue specimens not only confirms the upregulation of ITGA1, but also demonstrates a profound increase in pFAK staining when compared with healthy control sections. Additionally, a major proportion of the staining colocalizes with the CAV1 staining and thus confirms the in silico connections as suggested by STRING. Interestingly, in the healthy control sections, immunostainings for both ITGA1 and pFAK were restricted to the photoreceptor segments, whereas in ERU the staining intensity at the level of the OLM and additional staining throughout the tissue became evident (Fig. 4). Because focal adhesions are sites where integrins link the extracellular matrix (ECM) with the intracellular cytoskeleton, and additional upregulated proteins identified here include the typical intracellular focal adhesion proteins such as actinin-alpha 2 and 4, the observed upregulation at the level of the OLM suggests yet unknown active processes concomitant to photoreceptor degeneration and tissue remodeling occurring in ERU. Since the OLM is located opposite to the retinal pigment epithelium which is part of the outer blood-retinal barrier (31), this increase in focal adhesion kinase activity could indicate activation processes in connection to BRB break down. With respect to ECM proteins we found apart from ITGA1, ITGAV, ITGB1, and ITGB8 also upregulated in ERU. Interestingly, the  $\alpha V\beta 8$  integrin, combining ITGAV and ITGB8 subunits, has been shown to participate in activation of TGF $\beta$  by presenting it as so-called "latent complex" to cell surface metalloprotease MMP14, which in turn release diffusible TGF $\beta$  that can act in some distance from the site of activation (32). Because MMP14 was also included in our dataset among the upregulated proteins in ERU, this could suggest increased TGFB signaling in autoimmune uveitis. Although TGF $\beta$  is generally regarded as mediator of immune privilege, it is increased in the anterior eye chamber of mice in experimental autoimmune uveitis (EAU) (33). Likewise, increased expression of TGF $\beta$  had been observed in retinal tissue of Lewis rats developing EAU and it had been suggested to antagonise the proliferative action of similarly elevated VEGF on endothelial cells (34). Whether or not  $TGF\beta$  is increased in ERU retina as well and which are the functional implications will be the focus of our future studies.

Further ECM proteins that are upregulated in ERU comprise vitronectin (VTN) and fibronectin (FN). FN is multidomain molecule, containing both VEGF-binding domains as well as integrin-binding domains. Simultaneous binding of the pro-angiogenic growth factor VEGF and alpha5beta1 integrin to FN greatly enhances the pro-angiogenic effect of VEGF by increasing endothelial cell proliferation (35, 36). Since we have previously reported upregulation of VEGF by retinal Müller cells in the context of ERU pathology (37), the upregulation of VEGF-receptive ECM proteins in the retina may suggest a synergistic pathomechanism for VEGF in ERU.

The method applied here proved to be very valuable in enriching cell membrane proteins of small tissue samples. The identified pathways involved in retinal homeostasis as well as major changes associated with a spontaneous organ specific autoimmune disease led to a better understanding of uveitis related pathways. Further experiments will clarify the role of changed candidates involved in focal adhesions, ECM, and antigen processing to advance to a systematically understanding of disease pathogenesis.

# CONCLUSION

We aimed at increasing sensitivity for comparative proteomics screening of retina targeted by autoimmune uveitis. Changes in membrane proteins are especially interesting to understand initial events in tissue pathogenesis. Furthermore, because ERU pathology presents with a breakdown of the BRB, the strategy to enrich for membrane proteins proved additionally useful in depleting serum-derived proteins that would mask the detection of tissue-related changes. Another difficulty for comparative proteomics is added by the fact that the only available spontaneous animal model for this devastating disease is the horse and thus the clinical cases are based on an outbred population with a high variability. However, because this is a situation resembling the patient-topatient variability in humans, we tested whether it is feasible to perform instead a technically well-controlled proteomics comparison of single specimens and increase the caseload in the validation phase. This worked well because we could confirm the initially suggested regulation with all selected candidate proteins on tissue repositories. Thus, the high sensitivity of the proteomics comparison in combination with profound data mining enabled us to create new hypothesis for molecular pathways involved in ERU that can be validated and investigated in depth in the future.

Acknowledgments—We thank Caroline Bobe and Sandra Helm for excellent technical assistance and Marcel Blindert for scripting.

- \* This work was supported by a grant from the Bundesministerium für Bildung und Forschung (BMBF, SysTec-Verbund IMAGING FKZ 0315508A) and by the Deutsche Forschungsgemeinschaft (DFG) Grants SFB 571 A5 and DE 719/2-2.
  - S This article contains supplemental material.
  - ‡‡ Authors contributed equally to this work.
- \*\* To whom correspondence should be addressed: Department of Protein Science, Helmholtz Zentrum München, Ingolstädter Landstr. 1, D-85764 Neuherberg. Tel.: 00498931873941; Fax: 00498931874426; E-mail: hauck@helmholtz-muenchen.de.

## **REFERENCES**

- 1. Forrester, J. V. (1991) Uveitis: pathogenesis. Lancet 338, 1498-1501
- Martin, T. M., Smith, J. R., and Rosenbaum, J. T. (2002) Anterior uveitis: current concepts of pathogenesis and interactions with the spondyloarthropathies. Curr. Opin. Rheumatol. 14, 337–341
- Deeg, C. A., Hauck, S. M., Amann, B., Pompetzki, D., Altmann, F., Raith, A., Schmalzl, T., Stangassinger, M., and Ueffing, M. (2008) Equine recurrent uveitis—a spontaneous horse model of uveitis. *Ophthalmic. Res.* 40, 151–153
- Deeg, C. A. (2009) A proteomic approach for studying the pathogenesis of spontaneous equine recurrent uveitis (ERU). Vet. Immunol. Immunopathol. 128, 132–136
- Hauck, S. M., Schoeffmann, S., Amann, B., Stangassinger, M., Gerhards, H., Ueffing, M., and Deeg, C. A. (2007) Retinal Mueller glial cells trigger the hallmark inflammatory process in autoimmune uveitis. *J. Proteome* Res. 6, 2121–2131
- Zipplies, J. K., Hauck, S. M., Schoeffmann, S., Amann, B., Stangassinger, M., Ueffing, M., and Deeg, C. A. (2009) Serum PEDF levels are decreased in a spontaneous animal model for human autoimmune uveitis. *J. Pro*teome Res. 8, 992–998
- Caspi, R. R. (2002) Th1 and Th2 responses in pathogenesis and regulation of experimental autoimmune uveoretinitis. *Int. Rev. Immunol.* 21, 197–208
- Deeg, C. A., Kaspers, B., Gerhards, H., Thurau, S. R., Wollanke, B., and Wildner, G. (2001) Immune responses to retinal autoantigens and peptides in equine recurrent uveitis. *Invest. Ophthalmol. Vis. Sci.* 42, 393–398
- Nagaraj, N., Lu, A., Mann, M., and Wisniewski, J. R. (2008) Detergent-based but gel-free method allows identification of several hundred membrane proteins in single LC-MS runs. J. Proteome Res. 7, 5028–5032
- 10. Hauck, S. M., Gloeckner, C. J., Harley, M. E., Schoeffmann, S., Boldt, K.,

- Ekstrom, P. A., and Ueffing, M. (2008) Identification of paracrine neuro-protective candidate proteins by a functional assay-driven proteomics approach. *Mol. Cell. Proteomics* **7**, 1349–1361
- Olsen, J. V., de Godoy, L. M., Li, G., Macek, B., Mortensen, P., Pesch, R., Makarov, A., Lange, O., Horning, S., and Mann, M. (2005) Parts per million mass accuracy on an Orbitrap mass spectrometer via lock mass injection into a C-trap. *Mol. Cell. Proteomics* 4, 2010–2021
- Kamburov, A., Wierling, C., Lehrach, H., and Herwig, R. (2009) ConsensusPathDB-a database for integrating human functional interaction networks. *Nucleic Acids Res.* 37, D623–D628
- Maere, S., Heymans, K., and Kuiper, M. (2005) BiNGO: a Cytoscape plugin to assess overrepresentation of gene ontology categories in biological networks. *Bioinformatics* 21, 3448–3449
- Krogh, A., Larsson, B., von Heijne, G., and Sonnhammer, E. L. (2001) Predicting transmembrane protein topology with a hidden Markov model: application to complete genomes. *J. Mol. Biol.* 305, 567–580
- Jensen, L. J., Kuhn, M., Stark, M., Chaffron, S., Creevey, C., Muller, J., Doerks, T., Julien, P., Roth, A., Simonovic, M., Bork, P., and von Mering, C. (2009) STRING 8-a global view on proteins and their functional interactions in 630 organisms. *Nucleic Acids Res.* 37, D412–D416
- Ehrenhofer, M. C., Deeg, C. A., Reese, S., Liebich, H. G., Stangassinger, M., and Kaspers, B. (2002) Normal structure and age-related changes of the equine retina. Vet. Ophthalmol. 5, 39–47
- Morgan, J. M., Navabi, H., Schmid, K. W., and Jasani, B. (1994) Possible role of tissue-bound calcium ions in citrate-mediated high-temperature antigen retrieval. J. Pathol. 174, 301–307
- Baatz, M., Arini, N., Schape, A., Binnig, G., and Linssen, B. (2006) Objectoriented image analysis for high content screening: detailed quantification of cells and sub cellular structures with the Cellenger software. Cytometry A. 69, 652–658
- Baatz, M., Zimmermann, J., and Blackmore, C. G. (2009) Automated analysis and detailed quantification of biomedical images using Definiens Cognition Network Technology. Comb. Chem. High Throughput Screen 12, 908–916
- Albrethsen, J., Knol, J. C., Piersma, S., Pham, T. V., de Wit, M., Mongera, S., Carvalho, B., Verheul, H. M., Fijneman, R. J., Meijer, G. A., and Jimenez, C. R. (2010) Sub-nuclear proteomics in colorectal cancer: Identification of proteins enriched in the nuclear matrix fraction and regulation in adenoma to carcinoma progression. *Mol. Cell. Proteomics* 5, 988–1005
- Wade, C. M., Giulotto, E., Sigurdsson, S., Zoli, M., Gnerre, S., Imsland, F., Lear, T. L., Adelson, D. L., Bailey, E., Bellone, R. R., Blocker, H., Distl, O., Edgar, R. C., Garber, M., Leeb, T., Mauceli, E., MacLeod, J. N., Penedo, M. C., Raison, J. M., Sharpe, T., Vogel, J., Andersson, L., Antczak, D. F., Biagi, T., Binns, M. M., Chowdhary, B. P., Coleman, S. J., Della Valle, G., Fryc, S., Guerin, G., Hasegawa, T., Hill, E. W., Jurka, J., Kiialainen, A., Lindgren, G., Liu, J., Magnani, E., Mickelson, J. R., Murray, J., Nergadze, S. G., Onofrio, R., Pedroni, S., Piras, M. F., Raudsepp, T., Rocchi, M., Roed, K. H., Ryder, O. A., Searle, S., Skow, L., Swinburne, J. E., Syvanen, A. C., Tozaki, T., Valberg, S. J., Vaudin, M., White, J. R., Zody, M. C., Lander, E. S., and Lindblad-Toh, K. (2009) Genome sequence, comparative analysis, and population genetics of the domestic horse. Science 326, 865–867
- Hauck, S. M., Ekstrom, P. A., Ahuja-Jensen, P., Suppmann, S., Paquet-Durand, F., van Veen, T., and Ueffing, M. (2006) Differential modification of phosducin protein in degenerating rd1 retina is associated with constitutively active Ca2+/calmodulin kinase II in rod outer segments. *Mol. Cell. Proteomics* 5, 324–336
- Iandiev, I., Uckermann, O., Pannicke, T., Wurm, A., Tenckhoff, S., Pietsch, U. C., Reichenbach, A., Wiedemann, P., Bringmann, A., and Uhlmann, S. (2006) Glial cell reactivity in a porcine model of retinal detachment. *Invest. Ophthalmol. Vis. Sci.* 47, 2161–2171
- Iandiev, I., Tenckhoff, S., Pannicke, T., Biedermann, B., Hollborn, M., Wiedemann, P., Reichenbach, A., and Bringmann, A. (2006) Differential regulation of Kir4.1 and Kir2.1 expression in the ischemic rat retina. *Neurosci. Lett.* 396, 97–101
- Pannicke, T., Uckermann, O., landiev, I., Wiedemann, P., Reichenbach, A., and Bringmann, A. (2005) Ocular inflammation alters swelling and membrane characteristics of rat Muller glial cells. *J. Neuroimmunol.* 161, 145–154
- 26. Punzo, C., Kornacker, K., and Cepko, C. L. (2009) Stimulation of the

- insulin/mTOR pathway delays cone death in a mouse model of retinitis pigmentosa. *Nat. Neurosci.* **12**, 44–52
- Cresswell, P., Ackerman, A. L., Giodini, A., Peaper, D. R., and Wearsch, P. A. (2005) Mechanisms of MHC class I-restricted antigen processing and cross-presentation. *Immunol. Rev.* 207, 145–157
- Epperson, D. E., Arnold, D., Spies, T., Cresswell, P., Pober, J. S., and Johnson, D. R. (1992) Cytokines increase transporter in antigen processing-1 expression more rapidly than HLA class I expression in endothelial cells. *J. Immunol.* 149, 3297–3301
- Ma, W., Lehner, P. J., Cresswell, P., Pober, J. S., and Johnson, D. R. (1997) Interferon-gamma rapidly increases peptide transporter (TAP) subunit expression and peptide transport capacity in endothelial cells. *J. Biol. Chem.* 272, 16585–16590
- Gosens, I., den Hollander, A. I., Cremers, F. P., and Roepman, R. (2008) Composition and function of the Crumbs protein complex in the mammalian retina. Exp. Eye Res. 86, 713–726
- Crane, I. J., and Liversidge, J. (2008) Mechanisms of leukocyte migration across the blood-retina barrier. Semin. Immunopathol. 30, 165–177
- Sheppard, D. (2005) Integrin-mediated activation of latent transforming growth factor beta. Cancer Metastasis Rev. 24, 395–402
- Ohta, K., Wiggert, B., Yamagami, S., Taylor, A. W., and Streilein, J. W. (2000) Analysis of immunomodulatory activities of aqueous humor from

- eyes of mice with experimental autoimmune uveitis. *J. Immunol.* **164**, 1185–1192
- 34. Vinores, S. A., Chan, C. C., Vinores, M. A., Matteson, D. M., Chen, Y. S., Klein, D. A., Shi, A., Ozaki, H., and Campochiaro, P. A. (1998) Increased vascular endothelial growth factor (VEGF) and transforming growth factor beta (TGFbeta) in experimental autoimmune uveoretinitis: upregulation of VEGF without neovascularization. *J. Neuroimmunol.* 89, 43–50
- Wijelath, E. S., Rahman, S., Namekata, M., Murray, J., Nishimura, T., Mostafavi-Pour, Z., Patel, Y., Suda, Y., Humphries, M. J., and Sobel, M. (2006) Heparin-II domain of fibronectin is a vascular endothelial growth factor-binding domain: enhancement of VEGF biological activity by a singular growth factor/matrix protein synergism. Circ. Res. 99, 853–860
- Wijelath, E. S., Murray, J., Rahman, S., Patel, Y., Ishida, A., Strand, K., Aziz, S., Cardona, C., Hammond, W. P., Savidge, G. F., Rafii, S., and Sobel, M. (2002) Novel vascular endothelial growth factor binding domains of fibronectin enhance vascular endothelial growth factor biological activity. Circ. Res. 91, 25–31
- Deeg, C. A., Altmann, F., Hauck, S. M., Schoeffmann, S., Amann, B., Stangassinger, M., and Ueffing, M. (2007) Down-regulation of pigment epithelium-derived factor in uveitic lesion associates with focal vascular endothelial growth factor expression and breakdown of the blood-retinal barrier. *Proteomics* 7, 1540–1548